

## Controlling hysteresis in superconducting constrictions with a resistive shunt

This content has been downloaded from IOPscience. Please scroll down to see the full text.

2015 Supercond. Sci. Technol. 28 072003

(<http://iopscience.iop.org/0953-2048/28/7/072003>)

View [the table of contents for this issue](#), or go to the [journal homepage](#) for more

Download details:

IP Address: 134.100.109.113

This content was downloaded on 18/05/2015 at 13:26

Please note that [terms and conditions apply](#).

## Fast Track Communication

# Controlling hysteresis in superconducting constrictions with a resistive shunt

Nikhil Kumar<sup>1</sup>, C B Winkelmann<sup>2,3</sup>, Sourav Biswas<sup>1</sup>, H Courtois<sup>2,3</sup> and Anjan K Gupta<sup>1</sup>

<sup>1</sup> Department of Physics, Indian Institute of Technology Kanpur, Kanpur 208016, India

<sup>2</sup> Université Grenoble Alpes, Institut Néel, F-38042 Grenoble, France

<sup>3</sup> CNRS, Institut Néel, F-38042 Grenoble, France

E-mail: [knikhil@iitk.ac.in](mailto:knikhil@iitk.ac.in)

Received 24 March 2015, revised 24 April 2015

Accepted for publication 28 April 2015


Published 18 May 2015



CrossMark

## Abstract

We demonstrate control of the thermal hysteresis in superconducting constrictions by adding a resistive shunt. In order to prevent thermal relaxation oscillations, the shunt resistor is placed in close proximity to the constriction, making the inductive current-switching time smaller than the thermal equilibration time. We investigate the current–voltage characteristics of the same constriction with and without the shunt-resistor. The widening of the hysteresis-free temperature range is explained on the basis of a simple model.

 Online supplementary data available from [stacks.iop.org/sust/28/072003/mmedia](http://stacks.iop.org/sust/28/072003/mmedia)

Keywords: superconducting constrictions, micro-SQUIDs, hysteresis

(Some figures may appear in colour only in the online journal)

## 1. Introduction

A superconducting weak-link (WL), such as a constriction, between two bulk superconductors is of interest for its Josephson junction-like properties and subsequent application to micron size superconducting quantum interference devices ( $\mu$ -SQUIDs) [1, 2]. The latter can be used in probing magnetism at small scales [3–6]. Hysteresis present in current–voltage characteristics (IVCs) is a limiting factor in WL-based SQUIDs. In a hysteretic IVC when the current is ramped up from zero, the device typically switches to a non-zero voltage state at the critical current  $I_c$ . The subsequent current ramp-down gives a switching to zero-voltage state at a smaller current, called re-trapping current  $I_r$ . Hysteresis in IVCs is seen at low temperatures and disappears above a crossover temperature  $T_h$  as  $I_c$  and  $I_r$  meet [7–9]. In a conventional tunnel-barrier type Josephson junction, hysteresis arises from large junction capacitance and can be eliminated by adding a shunt resistor in parallel to the junction [1, 10]. The effect of the shunt resistor on nano-wire based WL devices was modeled recently using a resistively and capacitively shunted

junction (RCSJ) model with an effective capacitive time [11]. The hysteresis in similar devices is well understood using the thermal model [12]. The hysteresis in WLs is due to local Joule-heating [13, 14], which gives rise to a self-sustained resistive hot-spot in the WL region, even below  $I_c$ .

Eliminating thermal hysteresis in WLs has been the subject of intense research in the past years. A normal metal shunt directly on top of the constriction [15–17] has been tried, but it affects both the superconductivity and thermal properties in a way that depends on the interface transparency. Using a bilayer with a superconductor (that can be locally etched with a focused ion beam) covering a normal metal film allows one to obtain a WL that is also a good thermal bath [18]. A parallel shunt resistor far away from the WL [19] is a more flexible approach, but it gives rise to relaxation oscillations due to a large inductive time for switching of the current between the WL and the shunt. The performance of such SQUIDs with a distant shunt resistor is eventually similar to that of the hysteretic ones [3, 19]. A systematic study of the ability of a parallel shunt in preventing both the thermal runaway and hysteresis is thus highly desirable.

The role of a shunt resistor can be understood using a simple quasi-static thermal model discussed by Tinkham *et al* [12]. In this model, the heat generated in the resistive hot-spot in a long constriction is conducted (only) through electronic conduction to the large electrodes at the end. The thermal conductivity  $K$  of the normal metal and superconductor are assumed to be identical and temperature-independent. The re-trapping current is then found to be  $I_r(T_b) = I_r(0)\sqrt{1 - T_b/T_c}$  with  $I_r(0) = 4\sqrt{KAT_c/LR_n}$ . Here  $R_n$  is the normal resistance of the constriction of length  $L$  and cross-sectional area  $A$ ,  $T_b$  is the bath temperature and  $T_c$  is the superconductor critical temperature. From Ginzburg–Landau theory [2] the critical current follows  $I_c(T_b) = I_c(0)(1 - T_b/T_c)$  in the regime  $T_b > T_c/2$ . Thus  $I_c$  and  $I_r$  cross at a crossover temperature<sup>4</sup>  $T_h = T_c[1 - [I_r(0)/I_c(0)]^2]$ . In the presence of a shunt resistor  $R_s$ , the bias current is shared between the shunt and the WL when the latter is resistive. Thus, in the  $I_r(0)$  expression,  $1/R_n$  is replaced by  $(1/R_n) + (1/R_s)$ . As a result  $I_r(0)$  changes to a higher value given by

$$I_{rs}(0) = I_r(0)\sqrt{1 + R_n/R_s}. \quad (1)$$

In contrast,  $I_c$  remains unaffected. Hence the crossover temperature decreases and the hysteresis-free temperature range  $[T_h, T_c]$  widens thanks to the shunt. For eliminating hysteresis above temperature  $T$ ,  $R_s$  with value less than  $R_{sc} = R_n/[\{I_c(T)/I_r(T)\}^2 - 1]$  will be required. The assumed immediate sharing of the bias current between WL and  $R_s$  implies a small inductive current-switching time as compared to the thermal equilibration time. The minimum shunt resistor value,  $R_{sc}$ , from our simple model can also describe the behavior of shunted nano-wire devices studied by Brenner *et al* [11].

In this paper, we compare the current–voltage characteristics of carefully designed WL devices with (and without) a shunt resistor kept in close vicinity of the WL, thus making the inductive current-switching time smaller than the thermal equilibration time. We observe an increase in the re-trapping current and a widening of the hysteresis-free temperature range thanks to the shunt, which we discuss using the above model.

## 2. Experimental details

Devices were fabricated on Si substrates in two subsequent lithography and e-beam deposition steps as follows: (1) laser lithography of hatch patterned shunt resistor<sup>5</sup> and alignment marks on a photo-resist, (2) deposition and lift-off of a Ti (3 nm)/Au (20 nm) layer, (3) oxygen reactive-ion-etching

<sup>4</sup> This assumes the  $T_c$  of the WL to be the same as the adjacent superconducting structure, which is actually not true for our devices.  $T_h$  will get further reduced, widening the hysteresis free temperature range due to different  $T_c$  corresponding to  $I_c$  and  $I_{r1}$ , owing to the proximity effect [8].

<sup>5</sup> This topology of the shunt was used with a motive to study how the shunt resistance value changes the IVCs of the WL. Thus we had planned to cut various struts of the shunt using focussed ion beam (FIB) to modify the resistance value. However, the yield in this process was extremely poor and thus we decided to remove the shunt altogether.

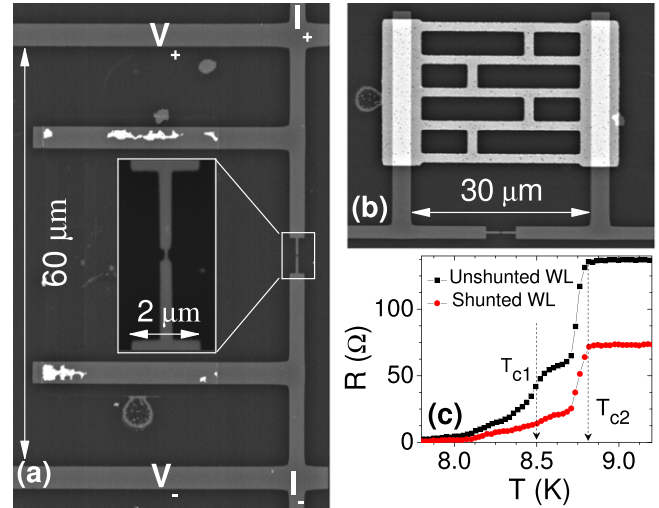


**Figure 1.** (a) SEM image of the WL device after etching the gold shunt. The inset in (a) shows the zoomed-in SEM image of the WL with patterned width 70 nm and length 150 nm. (b) SEM image of the same device rotated by 90°, before etching the hatch pattern shunt resistance made of gold microwires. (c) Resistance versus temperature (at 0.01 mA bias current) for the shunted and unshunted WLs, showing different transitions at  $T_{c1}$  and  $T_{c2}$  respectively corresponding to the narrow and the wide leads.

(RIE) to remove residual resist, (4) deposition of a 31 nm thick Nb-film, (5) aligned electron beam lithography of a PMMA resist of the WL pattern, (6) deposition and lift-off of a 20 nm thick Al-film, (7) etching of Nb with  $SF_6$ -RIE, (8) chemical removal of Al. After fully characterizing the shunted device, the Au shunt was etched using a  $KI-I_2$  solution which does not attack niobium. Electrical transport studies down to 1.3 K were pursued using a closed cycle He-refrigerator<sup>6</sup> with a homemade sample holder that incorporates copper powder filters. The data were recorded using data acquisition cards and homemade analog electronics. Two nominally identical devices demonstrated similar results.

## 3. Results and discussions

Figure 1 shows the electron micrograph and resistance versus temperature of the reported device. The WL (see inset of figure 1(a)) as designed has a length of 150 nm and a width of 70 nm. Narrow leads (width  $0.3 \mu\text{m}$ , length  $2.4 \mu\text{m}$ ) with normal resistance  $2R_1$ , connect symmetrically to the two ends of the WL of normal resistance  $R_{WL}$ . Wide leads of width  $2 \mu\text{m}$  connect the narrow leads to the shunt and the voltage probes. Figure 1(c) shows the measured resistance  $R$  versus temperature  $T$  before (see figure 1(b)) and after (see figure 1(a)) etching the Au shunt. For the two cases,  $R$  drops from a saturation value of 135 or  $72 \Omega$  (at 10 K) with two transitions at  $T_{c1} = 8.5 \text{ K}$  and  $T_{c2} = 8.8 \text{ K}$ . These two critical temperatures are attributed respectively to the narrow-leads and the wide leads. Let us stress that the critical temperatures  $T_{c1,2}$  are not affected by the removal of the Au shunt, which

<sup>6</sup> From ICE OXFORD.

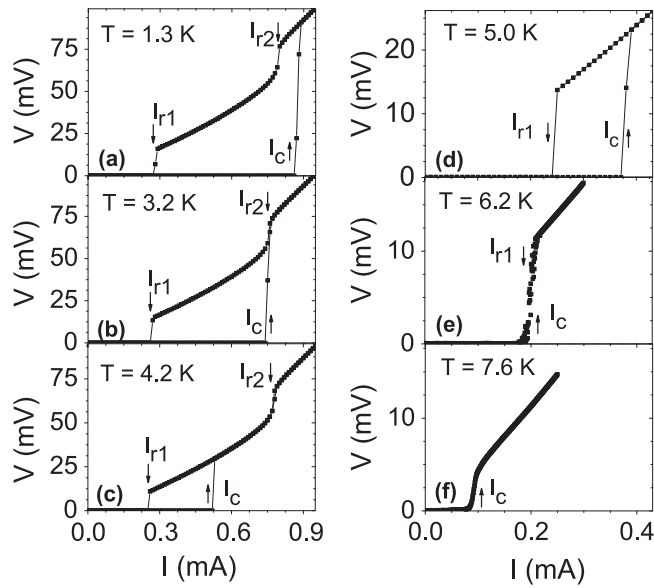


**Figure 2.**  $I$ - $V$  characteristics for the unshunted weak link at a set of different temperatures.

confirms that the shunt etching did not damage the niobium pattern. From the resistance drop at  $T_{c2}$  for the unshunted device, we find a square resistance  $R_{\square} = 3.5 \Omega$  giving a resistivity value of  $10.8 \mu\Omega \text{ cm}$  for the Nb film. From the narrow lead resistance and dimensions, we estimate  $R_{\text{WL}} = 9 \Omega$  and  $2R_1 = 56 \Omega$ . By comparing the resistances of the two devices just below  $T_{c2}$ , we find  $R_s = 35.6 \Omega$ , which is consistent with separate measurements of Au wires' resistances.

While designing the device, we have kept the shunt resistor close to the WL to minimize the associated loop-inductance  $L_{\text{sh}}$ . The inductance of a square loop with sides  $a$  and width  $b \ll a$ , is given by  $\frac{2}{\pi}\mu_0 a \ln[\frac{2a}{b}]$  [20]. Using this relation with  $a = 20 \mu\text{m}$  and  $b = 3 \mu\text{m}$ , we estimate the inductance of the loop containing gold shunt hatch pattern and the Nb leads as  $L_{\text{sh}} = 40 \text{ pH}$ . This gives an inductive-current-switching-time  $\tau_L = L_{\text{sh}}/(R_s + R_{\text{WL}}) \simeq 1 \text{ ps}$ . The heat is transferred to the substrate over a length-scale given by thermal healing length  $l_{\text{th}} (= \sqrt{Kt/\alpha} = 1.6 \mu\text{m})$  [8]<sup>7</sup>. Here  $t$  is the film thickness and  $\alpha$  is the interface heat loss coefficient. Thus the thermal cooling time is  $\tau_T = l_{\text{th}}^2/\pi^2 D = ct/\pi^2 \alpha$  with  $D (= K/c = 1 \text{ cm}^2 \text{ s}^{-1})$  as the diffusion constant and  $c$  as the volumetric heat capacity. We thus estimate the thermal time  $\tau_T = 2.5 \text{ ns}$ , which is much larger than  $\tau_L$ . When the WL switches from the superconducting to the resistive state, the current redistribution between the shunt and the WL is thus much faster than the thermal runaway in the device.

Figure 2 shows IVCs of the unshunted device at various temperatures. At low temperatures, sharp voltage jumps and drops are observed at the critical current  $I_c$  and at two retrapping currents  $I_{r1}$  and  $I_{r2}$ . The latter two arise from thermal instabilities respectively in the WL plus the narrow leads ( $I_{r1}$ ) and in the wide leads ( $I_{r2}$ ) [8]. At 1.3 K,  $I_c$  is higher than both  $I_{r1}$  and  $I_{r2}$  (see figure 2(a)). The IVC slope above  $I_{r2}$  is  $142 \Omega$ ,

<sup>7</sup> See the supplementary material for further details.

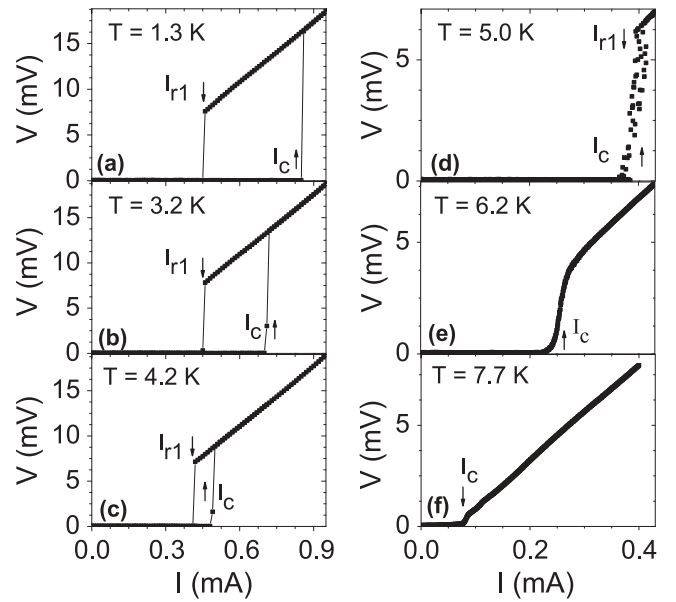


**Figure 3.**  $I$ - $V$  characteristics for the same weak-link device with a parallel shunt, at the same set of different temperatures as in figure 2.

slightly larger than the normal state value of  $135 \Omega$  because of over-heating. At higher temperatures when  $I_{r2}$  is smaller and heating less, the slope is  $135 \Omega$ . The IVC slope above  $I_{r1}$  is  $73 \Omega$ , which is close to the combined resistance  $R_{\text{WL}} + 2R_1$ , i.e.  $65 \Omega$ . The slightly larger value is due to the spread of the hot-spot into the wide leads. With increasing temperature,  $I_c$  crosses  $I_{r2}$  near 3.2 K (see figure 2(b)) and it merges with  $I_{r1}$  near  $T_h = 6.25 \text{ K}$  (see figure 2(e)). At higher temperature, the IVC is non-hysteretic and the resistance for  $I > I_c$  is  $65 \Omega$ , indicating that the WL as well as the narrow leads are resistive.

Figure 3 shows IVCs of the same device but prior to the shunt removal. We observe voltage jumps and drops at  $I_c$  and  $I_{r1}$  while the second retrapping current  $I_{r2}$  is visible only in IVCs with a larger bias current excursion<sup>7</sup>. In the resistive region, the slope is always  $22 \Omega$  which corresponds to the parallel combination of the normal resistance of the WL plus the narrow-leads with the shunt, i.e.  $(R_s^{-1} + (2R_1 + R_{\text{WL}})^{-1})^{-1}$ . The critical current  $I_c$  magnitude at low temperatures is the same, within the error bars, as that of the unshunted device, confirming that the shunt removal did not damage the WL. Remarkably, the re-trapping current  $I_{r1}$  has a higher value as compared to that of the unshunted device. As a result of  $I_{r1}$  enhancement,  $I_c$  and  $I_{r1}$  meet at a lower crossover temperature  $T_{\text{hs}} = 5 \text{ K}$  in the shunted device, see figure 3(d).

We summarize the temperature dependence of  $I_c$ ,  $I_{r1}$  and  $I_{r2}$  for both devices in figure 4. In every case, the retrapping current  $I_{r2}$  nearly follows a square root dependence with the bath temperature [8] extrapolating to zero at  $T_{c2}$ . This is consistent with  $I_{r2}$  being related to the thermal instability of the wide leads. Between about 3 K and the crossover temperature  $T_h$  or  $T_{\text{hs}}$ , the critical current  $I_c$  of both devices decreases linearly with temperature. The extrapolated critical temperature  $T_c$  close to 7.2 K is that of the WL itself. In both

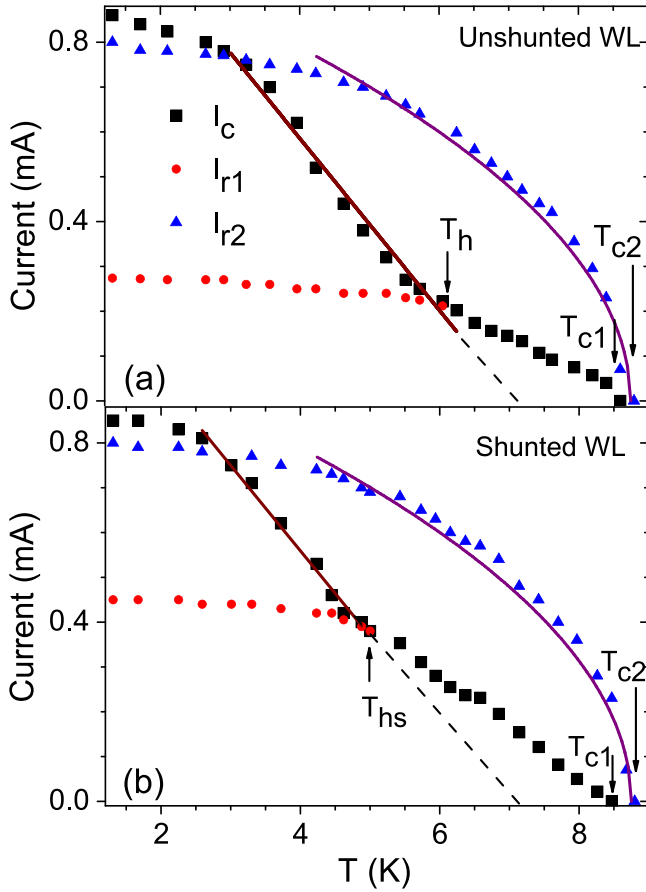


**Figure 4.** Temperature evolution of  $I_c$ ,  $I_{r1}$  and  $I_{r2}$  for (a) an unshunted weak link (WL) and (b) the same WL with a parallel shunt resistor, showing the reduction of crossover temperature in shunted case. The symbols are the data points. The continuous lines are the fits given by (in mA and K)  $I_c(T_b) = 0.18(7.2 - T_b)$  and  $I_{r2}(T_b) = 0.32(T_{c2} - T_b)^{1/2}$  for both the devices.

the devices, the critical current  $I_c$  decays markedly slower above  $T_h$  or  $T_{hs}$ , owing to the proximity effect [8].

The retrapping current  $I_{r1}$  follows a similar temperature dependence in the two devices but with a higher magnitude, by a factor of about 1.64, in the shunted device. This factor is similar to that found from equation 1, i.e. 1.67, by using  $R_s = 35.6 \Omega$  and  $R_n = 2R_1 + R_{WL} = 65 \Omega$ . A more appropriate model, incorporating the interface heat loss, for our device configuration provides a similar agreement, where the ratio is found to be close to 1.60<sup>7</sup>. For our devices, both the models give similar agreement<sup>7</sup> as the conduction dominates over interface heat loss because the narrow leads' length is comparable to  $l_{th}$  [8]. The two models have significant disagreement when the constriction is much longer than  $l_{th}$  (see footnote 7). Thanks to the shunt and the related  $I_{r1}$  enhancement, the hysteresis-free temperature range has increased from [6.25 K, 8.6 K] to [5 K, 8.6 K], see figure 4. For instance, the WL without shunt is hysteretic at 5 K, see figure 2(d), while the one with shunt is non-hysteretic, see figure 3(d).

The merging of  $I_c$  and  $I_{r1}$  above  $T_h$  is different from our earlier results on unshunted  $\mu$ -SQUIDs [8] where a crossing

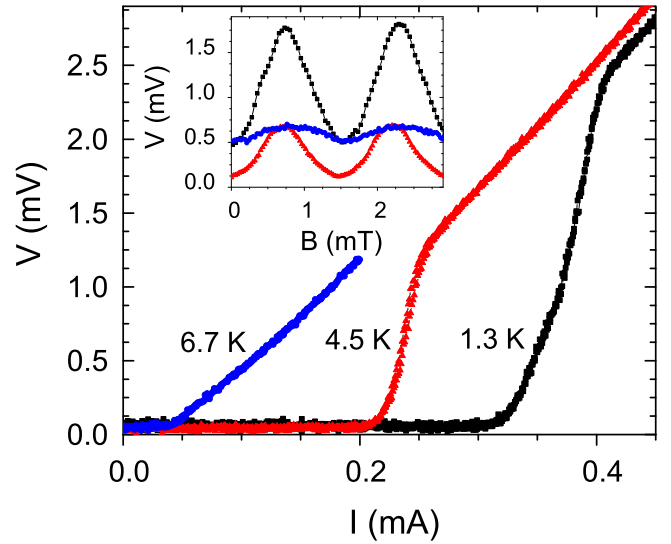


**Figure 5.** IVCs of a shunted  $\mu$ -SQUID at 1.3, 4.5, and 6.7 K showing non-hysteretic characteristics. The inset shows the SQUID oscillations at similar temperatures biased close to the critical current namely 0.37 mA for 1.3 K, 0.22 mA for 4.5 K and 0.05 mA for 6.7 K. The vertical scale at 6.7 K has been enhanced by a factor of 5 for better clarity in large scales.

of the two was seen at  $T_h$ . Due to the presence of the SQUID loop, the heat evacuation in the  $\mu$ -SQUIDs is more efficient. For single WL devices with similar  $I_c$  values, the less efficient heat evacuation favors merging over crossing. In fact, just below  $T_c$ , where  $I_c$  is small, heat evacuation eventually dominates, and we do see distinct signatures of both  $I_c$  and  $I_{r1}$  in IVCs. We also see large fluctuations in voltage close to  $T_h$  and for currents near  $I_c$  in both the devices, see figures 2(e) and 3(d). From the time-series data we find a bistable telegraphic-like voltage signal in this regime. Thus time averaged voltages in the IVCs show significant fluctuations. Close to the boundary of the bistable regime, more sensitivity to noise is indeed expected.

We have also studied a shunted  $\mu$ -SQUID device, with the same shunt geometry and resistance  $R_s$  value as in the single WLs discussed above. Although the critical current  $I_c$  is smaller in this SQUID due to the reduced width (<50 nm) of the weak links. The SQUID loop pattern is otherwise identical to our earlier work [8]. Figure 5 shows the IVCs of the shunted  $\mu$ -SQUID at different temperatures, which is found to be non-hysteretic down to 1.3 K. The expected  $T_h$  for this device without shunt is close to 3 K. This establishes the role of the shunt in widening the non-hysteretic temperature range for both WLs and  $\mu$ -SQUIDs. SQUID oscillations are clearly observed, see figure 5 inset.

Finally, let us discuss how we could further increase the re-trapping current and hence expand the hysteresis-free temperature range. Using a lower  $R_s$  value will increase  $I_{r1}$  further and widen the hysteresis-free temperature range for a given WL device. Nevertheless, this will also reduce the overall normal resistance and result in a lower voltage signal to be measured. The same can also be achieved by using a smaller  $I_c$  WL with same  $R_s$  value. We have verified this



claim in another shunted WL device, with the same  $R_s$  value and smaller  $I_c$ , showing a  $T_{hs}$  below 4.2 K. In any case, the shunt resistor has to be kept close enough to the WL, so as to avoid relaxation oscillations, but not too close to cause heat or electron sharing between WL and the shunt, which can affect the WL superconductivity.

#### 4. Conclusions

In summary, we have demonstrated a significant improvement of the hysteretic behavior of superconducting WLs and  $\mu$ -SQUIDS, using a parallel resistive shunt in close proximity to the WL. As a result of the shunt, the hysteresis-free temperature range is wider. Our results can help to further develop WL-based non-hysteretic devices such as SQUIDS.

#### Acknowledgments

Samples were fabricated at the platform Nanofab, CNRS Grenoble and measurements were carried out in IIT Kanpur. We thank Thierry Fournier for his help with sample fabrication. AKG thanks University Joseph Fourier for a visiting fellowship. NK acknowledges the financial support from CSIR, India. This work has been financed by the French Research National Agency, ANR-NanoQuartet (ANR12BS1000701) and the CSIR of the govt. of India.

#### References

- [1] Tinkham M 1996 *Introduction to Superconductivity* 2nd edn (New York: McGraw-Hill)
- [2] Likharev K K 1979 *Rev. Mod. Phys.* **51** 101
- [3] Wernsdorfer W 2001 *Adv. Chem. Phys.* **118** 99
- [4] Hasselbach K, Veauvy C and Mailly D 2000 *Physica C* **332** 140
- [5] Vasyukov D *et al* 2013 *Nat. Nanotechnology* **8** 639
- [6] Hao L, Macfarlane J C, Gallop J C, Cox D, Beyer J, Drung D and Schurig T 2008 *Appl. Phys. Lett.* **92** 192507
- [7] Hazra D, Pascal L M A, Courtois H and Gupta A K 2010 *Phys. Rev. B* **82** 184530
- [8] Kumar N, Fournier T, Courtois H, Winkelmann C B and Gupta A K 2015 *Phys. Rev. Lett.* **114** 157003
- [9] Blois A, Rozhko S, Hao L, Gallop J C and Romans E J 2013 *J. Appl. Phys.* **114** 233907
- [10] Clarke J and Braginski A I 2004 *The SQUID Handbook* vol 1 (Weinheim: Wiley)
- [11] Brenner M W, Roy D, Shah N and Bezryadin A 2012 *Phys. Rev. B* **85** 224507
- [12] Tinkham M, Free J U, Lau C N and Markovic N 2003 *Phys. Rev. B* **68** 134515
- [13] Skocpol W J, Beasley M R and Tinkham M 1974 *J. Appl. Phys.* **45** 4054
- [14] Courtois H, Meschke M, Peltonen J T and Pekola J P 2008 *Phys. Rev. Lett.* **101** 067002
- [15] Lam S K H and Tilbrook D L 2003 *Appl. Phys. Lett.* **82** 1078
- [16] Hazra D, Kirtley J R and Hasselbach K 2013 *Appl. Phys. Lett.* **103** 093109
- [17] Hazra D, Kirtley J R and Hasselbach K 2014 *Appl. Phys. Lett.* **104** 152603
- [18] Moseley R W, Booij W E, Tarte E J and Blamire M G 1999 *Appl. Phys. Lett.* **75** 262
- [19] Mück M, Rogalla H and Heiden C 1988 *Appl. Phys. A* **47** 285–9
- [20] Grover F W 1962 *Inductance Calculations: Working Formulas and Tables* (New York: Dover)